Research on Foot Trajectory Tracking of Parallel Wheel-legged Robot based on Dynamic Model Predictive Control

Daohe Liu
Beijing Institute of Technology https://orcid.org/0000-0001-5797-4760
Shoukun Wang (steelyliu@163.com)
Zhihua Chen
Beijing Institute of Technology
Junzheng Wang
Beijing Institute of Technology

Original Article

Keywords: Parallel mechanism, Trajectory tracking, Dynamics model, Model predictive control

Posted Date: June 30th, 2020

DOI: https://doi.org/10.21203/rs.3.rs-38159/v1

Research on foot trajectory tracking of parallel wheel-legged robot based on dynamic model predictive control

LIU Daohe[1,2], WANG Shoukun[1,2], CHEN Zhihua[1,2], WANG Junzheng[1,2]

(1. Key Laboratory of Complex System Intelligent Control and Decision, School of Automation, Beijing Institute of Technology, Beijing 100081, China;

2. Key Laboratory of Servo Motion System Drive and Control, School of Automation, Beijing Institute of Technology, Beijing 100081, China)

*Corresponding author: Shoukun Wang, steelyliu@163.com.

LIU Daohe: 3120180904@bit.edu.cn.

WANG Shoukun: steelyliu@163.com.

CHEN Zhihua: chen1314zh@163.com.

WANG Junzheng: wangjz@bit.edu.cn.

The postal address of the submitting author: No. 5, Zhongguancun South Street, Haidian District, Beijing, Beijing Institute of Technology, 100081.

Abstract: In this paper, the foot trajectory tracking control for parallel structure of the six wheel-legged robot is investigated. The accuracy of trajectory tracking and dynamic response with heavy load are the main challenges of parallel mechanism. To guarantee the tracking performance and improve dynamic response frequency to posture input, a method based on dynamic model predictive control is proposed under the establishment of dynamic model of single leg. Newton-Eulerian equation is derived and converted into a discrete state space expression for velocity loop control, appropriate parameters including prediction time domain, control time domain and proportional gain are determined by co-simulation. Desired sinusoidal trajectories with different frequencies are tracked with satisfactory performance in terms of accuracy and response frequency. Finally, comparative experimental results using BIT-NAZA robot derived from the proposed control strategy indicate that the delay error and amplitude error are better than PI controller under the same conditions. This research can provide theoretical and engineering guidance for accurate planning of intelligent robot, and facilitate the control performance of wheel-legged robot in practical system.

Keywords: Parallel mechanism; Trajectory tracking; Dynamics model; Model predictive control.

1. introduction

Parallel robots owns many advantages compared to serial robots, such as higher movement efficiency, higher load capacity, satisfactory precision and can reach a higher speed and acceleration [1]. Many researchers have been studying on those robot devices since the original Gough-Stewart parallel mechanism was developed by Gough and Stewart in 1954 and 1965, respectively [2-5]. The parallel structure of six wheel-legged robot developed in this paper named BIT-NAZA is shown in Fig.1, whose leg is composed of the Stewart platform inverted and mobile tires added to the bottom movable platform, which can realize wheel, foot and wheel-foot compound movements, and the payload can reach 400Kg.

Fig.1 Parallel structure of six wheel-legged robot

Trajectory tracking is the main challenge in practical applications for parallel platform because of its complicated dynamic and kinematic modeling. Two strategies named joint space control and task space control have been proposed to control a Stewart platform. In [6], the desired lengths of actuators of platform has been measured based on solving inverse kinetic problem of the desired trajectory in task space, which developed the joint space control. Task space control can be performed based on: (1) Position and rotation of the movable platform using position, orientation and vision sensors [7], (2) Solving forward kinematic problem (FKP) by the values of sensors [8]. The first approach is expensive and the latter method needs lots of calculations. In [9], according to a motion-tracking system, a vision-based control has been proposed for a 6-DoF parallel robot by measuring posture of movable platform. In [10], based on Homotopy Continuation approach, the nonlinear equations in FKP of a parallel robot were solved. Their method has been experienced in solving problem with high

precision.

Researchers have developed different control strategies in control of a 6-DOF Stewart Platform such as Linear Quadratic Gaussian (LQG) controller, Sliding-Mode controller, Robust approaches, PID controller, et al. In [11], by combining a Linear Quadratic Estimator (LQE) with a Li-near Quadratic Regulator (LQR), the LQG controller using reference position tracking has been proposed for motion control of a pneumatically-actuate 6-DoF platform. Meanwhile, the authors evaluated the robustness of the controller under different external disturbances in experimental tests. In [12], the trajectory tracking control of a 6-DoF pneumatically Stewart platform has been achieved by PID controller with feedback linearization. In the foregoing study, the controller's parameters were tuned by heuristic algorithm which was designed to solve non-convex problems. The work pressure has been controlled in inner control loop and the outer loop has been combined with displacement of the load under different external forces. Their analysis results were achieved in the Simulink of Matlab. An adaptive controller has been designed for the position tracking of a 6-DoF platform based on a linearized dynamic equations model. Two control loops have been employed and the PD controller and adaptive compensation have been combined by authors in [13]. In [14], the authors proposed a hybrid method based on Sliding Mode and Neural Networks, and a robust adaptive controller for a 6-DOF robot has been implemented without requiring inverse dynamic model. In [15], a robust adaptive controller has been designed according to task space dynamic equations. At last, a Stewart Platform was built in Simulink environment of MatLab software. The performance of controller for sinusoidal trajectory tracking was also evaluated. Sliding Mode control method has many advantages for control of robotic systems with large uncertain disturbances [16]. At present, vision-based methods have been widely researched for intelligent robots. In [17], a visual-based kinetic equations model of parallel platform has been designed by observing its legs measured by geometry of lines. The identification and control of platform were both simplified by proposed method. In [18], the vision servo system of parallel robots has been proposed based on hidden robot model by observing the leg directions.

In previous works, an observer-based robust controller [19] equipped with a fast friction estimator for a 6-DOF parallel electrical manipulator (PEM) in the joint-task space has been proposed. The cooperative control framework [20] is implemented in a host CPU and four slave CPUs for the four wheel-legged robot. In addition, an event triggered active disturbance rejection control (ADRC) of DC torque motors in position tracking problem has been propose in [21,22]. In this paper, a trajectory tracking control method for the foot of parallel wheel-legged robot based on dynamic model predictive control is proposed to improve the tracking accuracy and response rate of the foot to input posture. The main contributions of the paper are summarized as follows:

1) In order to improve the tracking accuracy and response frequency of the foot to the expected pose, consider the dynamic model of the platform established by the Newton-Euler equation under the loading condition and transform it into a discrete state space equation. Based on this, the prediction equation of the MPC controller is established and the optimal objective function is set to obtain the optimal control law.
2) Associated simulation to adjust the controllers of velocity and position loop to determine the appropriate control time domain, predicted time domain and other parameters. Comparative experimental results proved that the proposed method has more accurate performance in trajectory tracking, and the dynamic response effect is also better, which can provide theoretical and engineering guidance for the intelligent robot.

The remainder of the paper is organized as follow. Section 2 presents problem formulation and establishes the dynamic model of the Stewart platform. In section 3, MPC combined with the dynamic model establishes the platform's predictive equation, optimal objective function and solved optimal control amount. The simulation analysis and verification is discussed in section 4. The comparative experimental results are carried out in section 5 before a conclusion is drawn in section 6.

2. Platform modeling

The schematic diagram of the force on wheel-legged robot's single leg with load is shown in Figure 2. To simplify the analysis of the problem, the mass and rotational inertia of the single cylinder of each leg and the friction of the connecting part are ignored.

Assuming that the load mass is evenly distributed, *C* is the centroid of the load, and its coordinate in the inertial coordinate system *N* is R_c. $f_1 \sim f_6$ are the thrust generated by the six legs, and $\rho_1 \sim \rho_6$ are the vectors of the thrust of the center of mass *C* to the connection points between each leg and the movable platform. (for simplicity, only f_1 and ρ_1 are marked). The local coordinate system *B* uses the center of mass *C* as the origin and moves together with the load, and the inertial coordinate system *N* uses the center of the base platform as the origin.

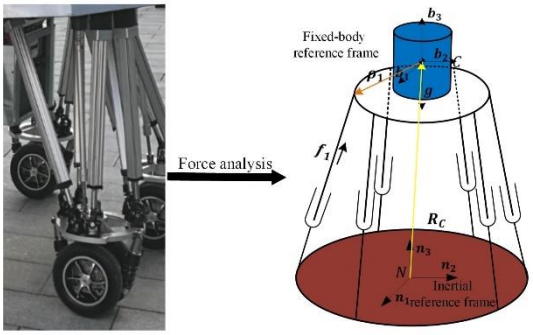

Fig.2 Force analysis of leg with load

The Newtonian equation of motion of the load center of mass in the inertial coordinate system N can be described as:

$$m\ddot{R}_C^N = \sum_{i=1}^{6} f_i^N + m g^N \tag{1}$$

Where R_C^N is the position coordinate of the center of load mass C in the inertial coordinate system N, $\ddot{R}_C^N$ is the acceleration vector of the center of load mass, f_i^N is the thrust vector of the i -th actuator, g^N is the acceleration vector of gravity, and m is the mass of load.

Then, Euler equation can be obtained by the torque analysis of the load in the local coordinate system B as follows:

$$J\dot{\omega}^B + \omega^B \times J\omega^B = \sum_{i=1}^{6} \rho_i^B \times f_i^B \tag{2}$$

Where ω^B is the angular velocity vector of the load represented by the local coordinate system B, f_i^B is the thrust vector of the i -th actuator, and the diagonal matrix J represents the principal moment of inertia of the load which uses the axes of the local coordinate system B as the inertia principal axes.

In order to transform the vector coordinates in the local coordinate system into the coordinates in the inertial coordinate system, a rotation matrix R is introduced as follows:

$$R = \begin{bmatrix} c\theta c\varphi & s\phi s\theta c\varphi - c\phi s\varphi & c\phi s\theta c\varphi + s\phi s\varphi \\ c\theta s\varphi & s\phi s\theta s\varphi + c\phi c\varphi & c\phi s\theta s\varphi - s\phi c\varphi \\ -s\theta & s\phi c\theta & c\phi c\theta \end{bmatrix}, RR^T = I_{3\times 3}$$

Where c and s represent the cosine and sine of the trigonometric function, ϕ, θ and φ are rotation angles of the load which rotates around the axes of the inertial coordinate system N. The rotation angular velocity of load, radial vector and coordinates of thrust vectors in the local coordinate system B can be represented as follows to the inertial coordinate system N.

$$\begin{aligned} \omega^B &= R^T \omega^N \\ \rho_i^B &= R^T \rho_i^N \\ f_i^B &= R^T f_i^N \end{aligned} \tag{3}$$

Substituting equation (3) into equation (2), the Euler equation in the inertial coordinate system can be described as:

$$JR^T\dot{\omega}^N + R^T\omega^N \times JR^T\omega^N = \sum_{i=1}^{6} R^T\rho_i^N \times R^T f_i^N \tag{4}$$

Considering that the rotation angular velocity ω^N and the radial thrust ρ_i^N are both vectors, the matrix of the components can be constructed as:

$$\Omega^N = \begin{bmatrix} 0 & -\omega_3^N & \omega_2^N \\ \omega_3^N & 0 & -\omega_1^N \\ -\omega_2^N & \omega_1^N & 0 \end{bmatrix}, P_i^N = \begin{bmatrix} 0 & -\rho_{i3}^N & \rho_{i2}^N \\ \rho_{i3}^N & 0 & -\rho_{i1}^N \\ -\rho_{i2}^N & \rho_{i1}^N & 0 \end{bmatrix}$$

The cross product (×) operation in Eulerian equation (4) can be replaced by a matrix operation, then the Eulerian equation (4) can be described as:

$$JR^T\dot{\omega}^N + R^T\Omega^N RJR^T\omega^N = \sum_{i=1}^{6} R^T P_i^N f_i^N \tag{5}$$

We can know that $f_i^N = n_i^N f_i$, n_i^N is the direct-ion vectors of thrust, f_i is the magnitude of thrust, then the both ends of equation (5) is multiplied by *R* at left, so the Euler equation and Newton 's equation of motion can be obtained as:

$$RJR^T\dot{\omega}^N + \Omega^N RJR^T\omega^N = \sum_{i=1}^{6} P_i^N n_i^N f_i \tag{6}$$

$$m\ddot{R}_C^N = \sum_{i=1}^{6} n_i^N f_i + mg^N \tag{7}$$

Assuming that the sampling period of control system is T_s, R, Ω^N, n_i^N are all constant in a single sampling period, discrete equations can be obtained by discretizing equations (6) and (7) as follows:

$$\dot{R}_C^N(k+1) = \dot{R}_C^N(k) + \frac{T_s}{m}\sum_{i=1}^{6} n_i^N f_i + T_s g^N \tag{8}$$

$$\omega^N(k+1) = \left(I_{3\times3} - T_s RJ^{-1}R^T\Omega^N RJR^T\right)\omega^N(k) + T_s RJ^{-1}R^T\sum_{i=1}^{6} P_i^N n_i^N f_i \tag{9}$$

From equation (8) and equation (9), the state space equation can be obtained as:

$$\begin{bmatrix} \dot{R}_C^N(k+1) \\ \omega^N(k+1) \end{bmatrix} = A_x \begin{bmatrix} \dot{R}_C^N(k) \\ \omega^N(k) \end{bmatrix} + T_s M_P^{-1} J_P \begin{bmatrix} f_1^N(k) \\ \mathrm{M} \\ f_6^N(k) \end{bmatrix} + T_s \begin{bmatrix} g^N \\ O_{3\times1} \end{bmatrix} \tag{10}$$

Where $A_x = \begin{bmatrix} I_{3\times3} & O_{3\times3} \\ O_{3\times3} & I_{3\times3} - T_s RJ^{-1}R^T\Omega^N RJR^T \end{bmatrix}$, $M_P = \begin{bmatrix} mI_{3\times3} & O_{3\times3} \\ O_{3\times3} & RJR^T \end{bmatrix}$, $J_P = \begin{bmatrix} n_1^N & \mathrm{L} & n_6^N \\ P_1^N n_1^N & \mathrm{L} & P_6^N n_6^N \end{bmatrix}$.

It is known that the variables $\begin{bmatrix} \dot{R}_C^N & \omega^N \end{bmatrix}^T$ and the actuator velocity vector $\dot{l}_1 \ \mathrm{L} \ \dot{l}_6^T$ have the following relation:

$$\begin{bmatrix} \dot{l}_1 \\ \mathrm{M} \\ \dot{l}_6 \end{bmatrix} = J_P^T \begin{bmatrix} \dot{R}_C^N \\ \omega^N \end{bmatrix} \tag{11}$$

So the equation (10) can be transformed into:

$$\begin{bmatrix} \dot{l}_1(k+1) \\ \mathrm{M} \\ \dot{l}_6(k+1) \end{bmatrix} = J_P^T A_x J_P^{-T} \begin{bmatrix} \dot{l}_1(k) \\ \mathrm{M} \\ \dot{l}_6(k) \end{bmatrix} + T_s J_P^T M_P^{-1} J_P \begin{bmatrix} f_1^N(k) \\ \mathrm{M} \\ f_6^N(k) \end{bmatrix} + T_s J_P^T \begin{bmatrix} g^N \\ O_{3\times1} \end{bmatrix} \tag{12}$$

Finally, we can think that the state vector is $x_p(k) = \dot{l}_1(k) \ \mathrm{L} \ \dot{l}_6(k)^T$, control vector is $u(k) = \begin{bmatrix} f_1^N(k) & \mathrm{L} & f_6^N(k) \end{bmatrix}^T$, and measurable disturbance vector is $v(k) = \begin{bmatrix} g^N & O_{3\times1} \end{bmatrix}^T$, $A_{xk} = J_p^T A_x J_p^{-T}$, $B_{uk} = T_s J_p^T M_p^{-1} J_p$, $B_{vk} = T_s J_p^T$, then the state equation can be described as:

$$x_p(k+1) = A_{xk}x_p(k) + B_{uk}u(k) + B_{vk}v(k) \tag{13}$$

The output equation can be written as

$$y_p(k) = x_p(k) \tag{14}$$

3. Controller development

3.1 The principle of control to platform

The block diagram of control structure of the leg of parallel wheel-legged robot is shown in Fig.3. The

position tracking of movable platform of Stewart platform to the input is realized by the double closed loop of the position and velocity. The inner loop is velocity loop, with the MPC controller used, the position loop adopts proportional and feedforward controller, it's used as outer loop. Based on the dynamic model of the Stewart platform, the MPC controller implements velocity control of the actuator through target velocity, actual velocity and prediction model of the leg. The expected length of actuator can be obtained by inverse kinematics of the input position vector and compared with the actual length of the integrator output. The deviation value is used as input signal of the MPC controller after being superimposed by the proportional controller and the feedforward differential signal. The velocity measurement value of outrigger of Stewart platform in the inner loop is fed back to the MPC controller, its output is obtained by the integrator to obtain the actual length of the outrigger, and then the posture output of the Stewart platform is obtained through the positive kinematics, so as to realize the tracking of actuator's velocity and posture of platform.

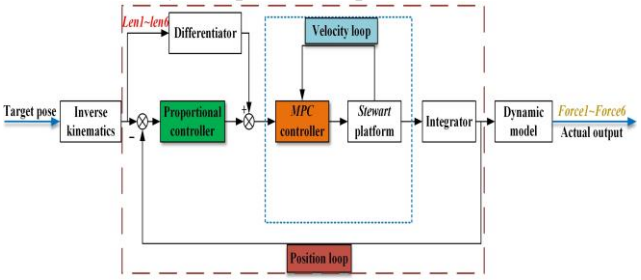

Fig.3 Control diagram of single leg

3.2 Establishment of the prediction model

The Stewart platform uses MPC controller for closed-loop velocity control. Its basic control structure is shown in Figure 4. Taking the velocity of each leg of the Stewart platform as the target vector $y_r(k)$. The state vector $x_c(k)$ of the controller is obtained by estimating the state vector $x_p(k)$ of the platform, and the output vector $y(k)$ in the prediction time domain of the Stewart platform is obtained from the prediction model. The control vector $u(k)$ is solved according to the optimized objective function and constraint conditions, and then $u(k)$ is input to the actuators to realize the tracking of the output vector $y_p(k)$ to the target vector $y_r(k)$.

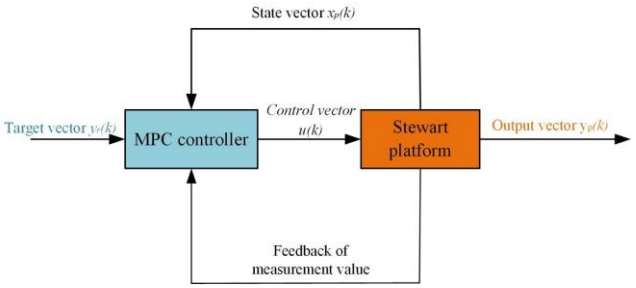

Fig.4 MPC controller and velocity loop control

From the dynamic models (13) and (14) derived from the foregoing, the state observer equation (15) can be obtained as follows:

$$\begin{cases} x_c(k+1) = A_{xk}x_c(k) + B_{uk}u(k) + B_{vk}v(k) \\ y(k) = x_c(k) \end{cases} \tag{15}$$

Where $x_c(k)$ takes the value of $x_p(k)$, A_{xk}, B_{uk} and B_{vk} are updated at every control cycle and remain constant in the predication domain p.

After establishing the prediction model, the first prediction state can be obtained as follows:

$$x_c(k+1) = A_{xk}x_c(k|k) + B_{uk}u(k) + B_{vk}v(k), k = 1$$

The prediction state of i -th step with update is as follows:

$$x_c(k+i|k) = A_{xk}x_c(k+i-1|k) + B_{uk}u(k+i-1|k) + B_{vk}v(k), 2 \le i \le p \tag{16}$$

The prediction output of i -th step can be obtained as follows:

$$y(k+i|k) = x_c(k+i|k), 1 \le i \le p \tag{17}$$

3.2 The cost function and its constraints

To achieve the optimal control effect, setting the objective function and minimize it. The expression of the optimization objective function can be de-scribed as follows:

$$J(\varepsilon, \Delta u_k) = \sum_{i=1}^{p} \left\| y(k+i|k) - y_r(k+i|k) \right\|_Q^2 + \sum_{i=1}^{m-1} \left\| \Delta u(k+i|k) \right\|_R^2 + \rho\varepsilon^2 \tag{18}$$

Where $y_r(k+i|k)$ is the target value in the pre-diction domain p starting from the current time *k*, which can be obtained by the target trajectory in the prediction time domain *p*, among this:

$$\Delta u_k = \left[\Delta u(k|k)^T \quad \Delta u(k+1|k)^T \quad \mathrm{L} \quad \Delta u(k+m|k)^T \right]^T \tag{19}$$

Where $\Delta u_k(k+i|k) = u(k+i|k) - u(k+i-1|k)$ is the difference between the control vectors at two sequential moments. The control domain *m* satisfies $m<p$, Q and R is weight matrices. The former item on the right side of equation (18) reflects the requirement for target performance tracking, and the latter item reflects the requirement for the change in control amount. In addition, by adding the relaxation factor, it can be guaranteed that the feasible solution can be obtained if the cost function violates the constraints, and the relaxation factors $\varepsilon > 0$ and ρ is the weight.

In practical systems, constraints on the amount of actuating signal and the output of the actuators are often required, so the output signal of actuators can be described as follows:

$$y_{\min}(k+i|k) - \varepsilon v_{\min} \le y(k+i|k) \le y_{\max}(k+i|k) + \varepsilon v_{\max}, 0 \le i \le m-1 \tag{20}$$

The constraint of actuating is as follows:

$$u_{\min}(k+i|k) \le u(k+i|k) \le u_{\max}(k+i|k), 0 \le i \le m-1 \tag{21}$$

The constraint of actuating signal change is as follows:

$$\Delta u_{\min}(k+i|k) \le \Delta u(k+i|k) \le \Delta u_{\max}(k+i|k), 0 \le i \le m-1 \tag{22}$$

Where $y_{\max}(k+i|k)$ and $y_{\min}(k+i|k)$ are the maximum and minimum values of the controlled object, $v_{\max} > 0$ and $v_{\min} > 0$ are the softening constraint vectors; $u_{\max}(k+i|k)$ and $u_{\min}(k+i|k)$ are the maximum and minimum values of the control signal; $\Delta u_{\max}(k+i|k)$ and $\Delta u_{\min}(k+i|k)$ are the maximum and minimum values of the control signal change.

3.3 Solving the objective optimization function

Equation (18) can be transformed as follows:

$$J(\varepsilon, \Delta u_k) = \rho\varepsilon^2 + \Delta u_k^T K_{\Delta u} \Delta u_k + 2\left(\begin{bmatrix} y_r(k+1|k) \\ \mathrm{M} \\ y_r(k+p|k) \end{bmatrix}^T K_{y_r} + v(k)^T K_v + u(k-1)^T K_u + x(k)^T K_x \right) \Delta u_k + const \tag{23}$$

Where $K_{\Delta u}$, K_{y_r}, K_v, K_u and K_x are all constant matrices, $const$ is a constant scalar, and $u(k-1)$ is the actuating signal at a moment before *k*. The minimization problem is transformed into a quadratic programming (*QP*) problem with constraints, which can obtain the optimal control increment sequence in the control domain.

$$\Delta u_k^* = \left[\Delta u^*(k|k)^T, \Delta u^*(k+1|k)^T, \mathrm{L}, \Delta u^*(k+m-1|k)^T \right]^T \tag{24}$$

Each time the control cycle is updated, the first element of this control sequence is added to $u(k-1)$ to obtain the optimal control amount at time *k*, so the control amount can be obtained as:

$$u(k) = u(k-1) + \Delta u^*(k|k) \tag{25}$$

4. Simulation results

The simulation model block diagram in MATLAB / SIMULINK from the control structure diagram of Fig.3 is established, as shown in Figure 5. Equations (13) and (14) are included in the dynamic model, and the MPC controller completes the predicted

output and optimal solution of the control variables. Create a model of the Stewart platform in the dynamic analysis software Adams and export it as an executable file in the Matlab environment, the control amount of the MPC controller is input to the model, at the same time, the measurements of length and velocity of each leg of the platform is fed back to the position loop controller and dynamic model. The step input is used to tune MPC in velocity loop and the sine-wave input is used to tune proportional controller in position loop.

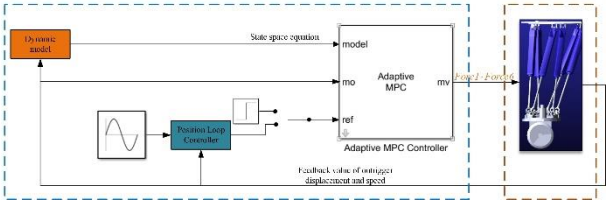

Fig.5 Control block diagram in Simulink

The main parameters of kinematics and dynamics of the Stewart platform established in Adams are shown in Table 1. Simulation and controller tuning are performed in the order of speed loop and position loop, and the sampling time T_s is set to 0.0005s.

Tab 1 The main parameters of Adams model

Parameter	Data	Unit
Mass of load	6.422	Kg
Principal moment of inertia	$\begin{bmatrix} 0.3246 & 0 & 0 \\ 0 & 0.3246 & 0 \\ 0 & 0 & 0.6439 \end{bmatrix}$	Kg·m^2
Top diameter	340	mm
Base diameter	488	mm
Height of top	976	mm
Static friction coefficient	0.1	/
Dynamic friction coefficient	0.05	/
Friction force preload	10	N

4.1 parameter tuning of velocity loop

The step signal with amplitude 0.15m/s is input to the MPC controller, and the constraint range of the actuating signal is ±700 N. In figure 6, the predication domain m=2 and the control domain p is variable. And in figure 7, the predication domain p=5 and the control domain m is variable.

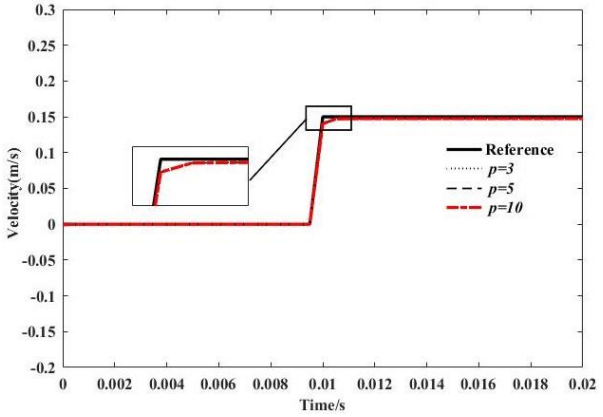

(a) Step response for m=2 and variable p

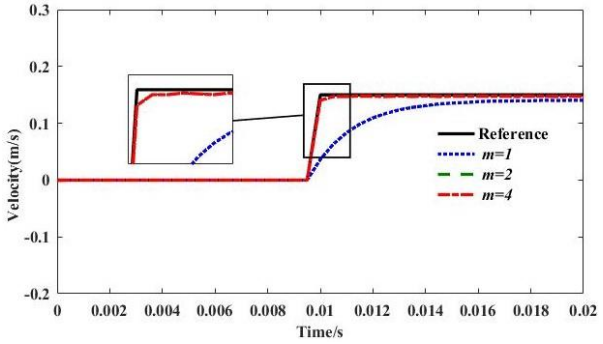

(b) Step response for p=5 and variable m

Fig.6 Step response for variable p and m

It can be seen from Fig. 6 that the change in the predicted time domain $\boldsymbol{p}$ has little effect on the step response, while the change in the control time domain $\boldsymbol{m}$ has a significant effect on the step response. Table 2 summarizes the step response when $\boldsymbol{m}$ changes.

Tab 2 Step response for p=5 and variable m

Test condition(p=5)	Rising time / s	Overshoot / %	Steady-state relative error / %
$m=1$	0.0035	0	-6
$m=2$	<0.0005	0	-1.7
$m=4$	<0.0005	0	-1.7

The analysis of Table 2 shows that as m increases, the step response rising time decreases, and the steady-state relative error decreases. Considering that if m increases, the amount of calculation will also increase, which is not conducive to the real-time nature of system control, therefore, choosing p=5 and m=2 as the MPC controller parameters can ensure the control performance while avoiding the increase of the control calculation time caused by the excessive value of m.

4.2 Position loop simulation and tuning of proportional controller

Next, tune the gain of the position loop proportional controller. The sine signal with frequency 2Hz and amplitude 0.15rad is used as the input signal to the position loop, and m=2, p=5 of the MPC controller are known. By gradually increasing the gain of the proportional controller, at last a proper gain 0.12 is obtained without oscillation. The experimental results shown in Fig.7. (a) is the sinusoidal response of the pitch axis attitude; (b) is the actuating signal of 6 actuators.

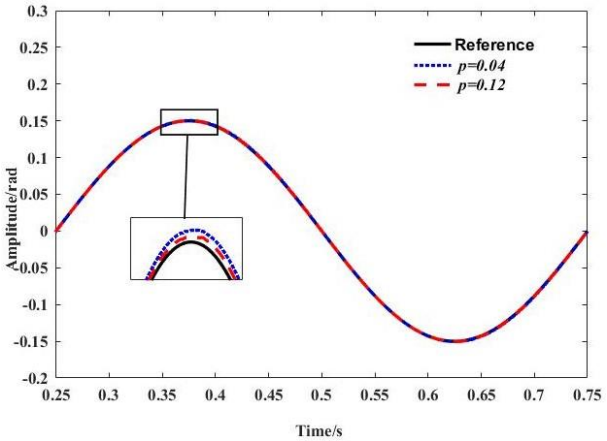

(a) Sinusoidal response

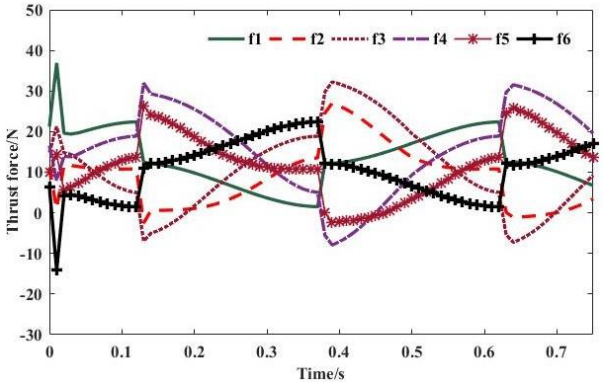

(b) Thrust force of actuator

Fig.7 Sine wave response for m=2, p=5

From the curve shown in Fig.7(a) we can know that the amplitude error of the sinusoidal response is 0.0004*rad* and the delay error is 0.0005s. It can be seen from Fig.7(b) that under the conditions of the parameters in Table 1, the thrust forces of actuators of the Stewart platform are all in the range of -15N ~ 40N, and the thrust forces change smoothly and continuously throughout the entire motion cycle of the platform, which can provide theoretical and engineering guidance for the selection of actuators of the Stewart platform.

Both simulation results can meet the need of accuracy. Therefore, the parameters of the MPC controller and the position loop controller gain 0.12 are used as the controller parameter for the next experiment.

5. Experimental results

The framework of robot distributed system is shown in Fig.8. The communication network includes TCP/IP based network, CAN bus network, RS232 communication network etc. The robot status information is sent to a monitor computer by wireless UDP transmission technology when the robot is working. There are five nodes on the CAN bus. Host CPU is the master node; slave CPUs are the slave nodes.

The actuator of the Stewart platform used in the experiment is an electric cylinder, which is driven by a servo motor. The main control computer at the bottom is equipped with a multi-core processor and has a PC/104 interface and runs in the Simulink/Real-Time environment. The upper-layer development computer writes the control algorithm and compiles it, and then sends it to the bottom-level master computer. The target computer uses the D/A converter card to convert the control digital to analog input to the Stewart platform actuator servo driver, and reads the speed information of the electric cylinder from the servo driver through the encoder interface.

The walking trajectory of the wheel-legged hexapod robot is shown in Fig.9. The accurate tracking to expected posture of the foot ensures that it meets the foot drop planning, decreases the cumulative error during the all walking process to ensure the adaptability of the wheel-legged robot to complex terrain. The experiment was carried out in the order of the attitude and displacement tracking test, and the comparative experiment was performed with the PI controller.

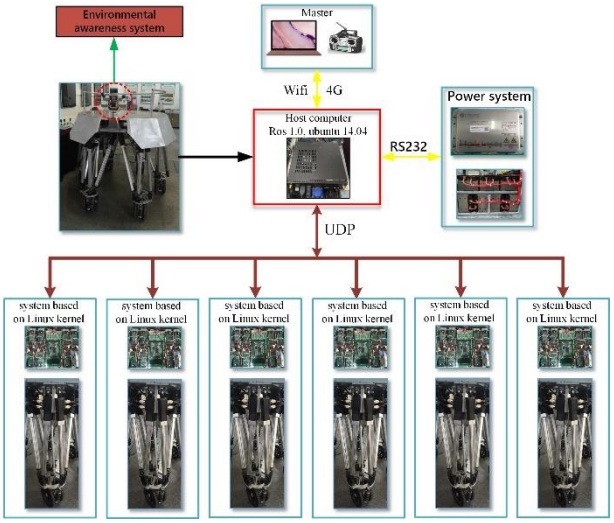

Fig.8 Framework of robot distributed system

Fig.9 Trajectory tracking of the single leg

First, an attitude tracking experiment is performed, and a sine wave signal is selected as the attitude input of the pitch axis. The frequencies are 1Hz, 2Hz, and 4Hz, and the amplitude is 0.0873rad. The PI controller with parameters P=25 and I=0.1 is applied in the comparative experiment. The experimental curve is shown in Fig.9, and the tracking performance comparison of MPC controller and PI controller is shown in Table 3.

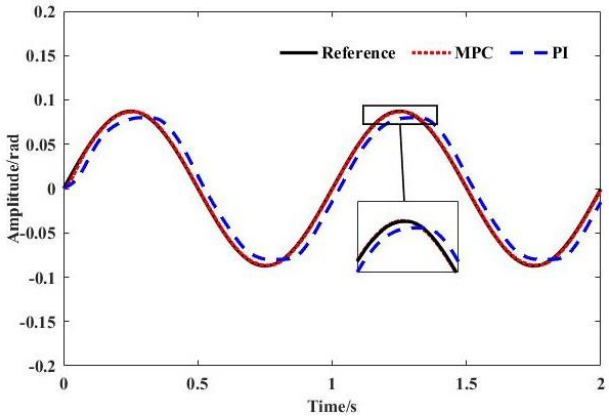

(a) Frequency 1Hz, Amplitude 0.0873Rad

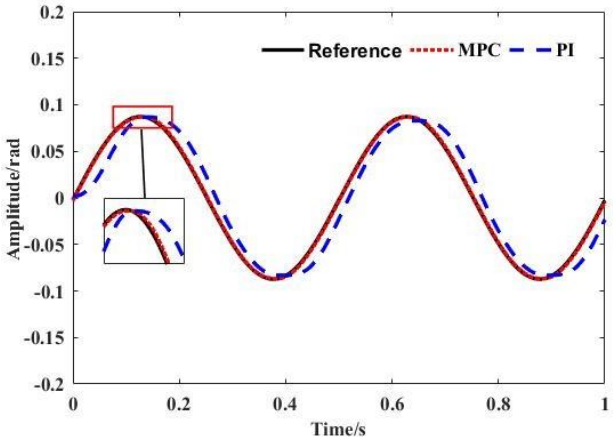

(b) Frequency 2Hz, Amplitude 0.0873Rad

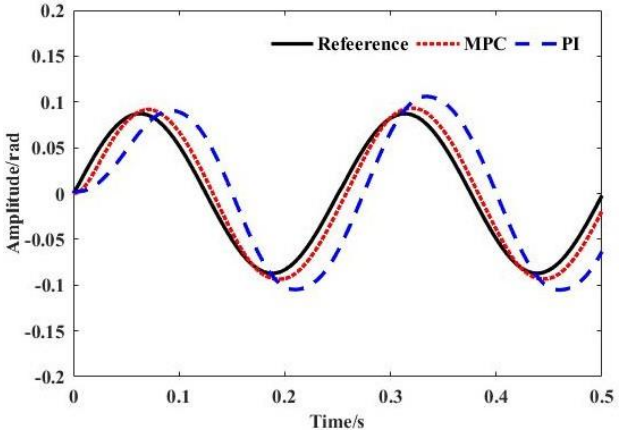

(c) Frequency 4Hz, Amplitude 0.0873Rad

Fig.10 Attitude tracking comparison between MPC controller and PI controller

Tab 3 Attitude tracking performance comparison

Frequency/*Hz*	Delay/*s*		Amplitude error/*rad*	
	MPC	PI	MPC	PI
1	0.0015	0.025	-0.0008	-0.0074
2	0.001	0.016	0.0004	-0.0004
4	0.006	0.022	0.0061	0.0189

The next step is a trajectory tracking experiment, as shown in Fig.9, the arch width (AC) of the cycloid is 320mm, the arch height (the distance from B to AC) is 80mm, and the arc ABC movement time is 3s. The results in Fig.10 show that the cycloidal trajectory tracking accuracy of the MPC controller is significantly better than that of the PI controller.

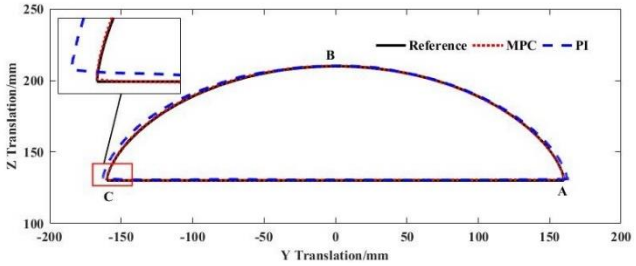

Fig.11 Displacement tracking comparison between MPC controller and PI controller

It can be known from the table 3 and table 4 that MPC controller is superior to the PI controller in terms of tracking accuracy and dynamic characteristics. Because the MPC controller takes into account the prediction model of the Stewart platform and adds optimized control, it can use the historical information of the controlled object to predict the future control amount changes, so it can guarantee more accurate tracking performance and adaptation.

6. Conclusions

This paper addressed the trajectory tracking control of a 6-DOF platform used as leg of the developed six parallel wheel-legged robot. At present, the research method of Stewart platform considered dynamic model combined with MPC controller is relatively rare, this paper investigates the dynamic model predictive control for foot trajectory tracking of the six wheel-legged robot. A control-close loop was designed based on two control loops including outer position loop used proportional controller and inner velocity loop used MPC controller. Furthermore, trajectory tracking control of the robot's foot-end was performed for different desired trajectories which resulted in an appropriate performance in tracking. From the experimental results, it can be inferred that the proposed method can be employed for trajectory tracking control of the 6-DOF parallel robot, which can provide theoretical and engineering guidance for practical robot application. As ongoing works, to further improve the control accuracy and stability to external disturbances such as the internal-robot friction and external-robot and environment interaction forces, et al.

References

[1] J.-P. Merlet, Parallel Robots, 74 Springer Science & Business Media, 2012.

[2] Davliakos, I.,&Papadopoulos,E.(2008). Model-based control of a 6-dof electro-hydraulic Stewart–Gough platform. Mechanism andMachineTheory, 43(11),1385-1400.

[3] Dasgupta, B. and T.S. Mruthyunjaya, The Stewart platform manipulator: a review. Mechanism and Machine Theory, 2000. 35(1): p. 15-40.

[4] Lee, S., et al., Position control of a Stewart platform using inverse dynamics control with approximate dynamics. Mechatronics, 2003. 13(6): p. 605-619.

[5] Ting, Y.,Chen,Y.S.,&Jar,H. C.(2004). Modeling and control for a Gough-Stewart platform CNC machine. Journal of Robotic System, 21(11),609-623

[6] J.H. Machiani, M.T. Masouleh, A. Kalhor, M.G. Tabrizi, F. Sanie, Control of a pneumatically actuated 6-dof Gough-Stewart platform, Proceedings of the Second RSI/ISM International Conference on Robotics and Mechatronics (ICRoM), (2014), pp. 166–171.

[7] J. Cazalilla, M. Vallés, Ángel Valera, V. Mata, M. Díaz-Rodríguez, Hybrid force/position control for a 3-dof 1t2r parallel robot: implementation, simulations and experiments, Mech. Based Des. Struct. Mach. 44 (1,2) (2016) 16–31.

[8] S.-K. Song, D.-S. Kwon, Efficient formulation approach for the forward kinematics of 3–6 parallel mechanisms, Adv. Rob. 16 (2) (2002) 191–215.

[9] R. Chellal, L. Cuvillon, E. Laroche, Model identification and vision-based h position control of 6-dof cable-driven parallel robots, Int. J. Control 90 (4) (2017) 684–701.

[10] A. Salimi Lafmejani, A. Kalhor, M. Tale Masouleh, A new development of homotopy continuation method, applied in solving nonlinear kinematic system of equations of parallel mechanisms, Proceedings of the Third RSI International Conference on Robotics and Mechatronics (ICROM), (2015), pp. 737–742.

[11] K.S. Grewal, R. Dixon, J. Pearson, LQG controller design applied to a pneumatic Stewart-Gough platform, Int. J. Autom. Comput. 9 (1) (2012) 45–53.

[12] D. Pršić, N. Nedić, V. Stojanović, A nature inspired optimal control of pneumaticdriven parallel robot platform, Proc. Inst. Mech. Eng. Part C J. Mech. Eng. Sci. 231 (1) (2017) 59–71.

[13] Q. Zhao, N. Wang, B.F. Spencer Jr, Adaptive position tracking control of electrohydraulic six-degree-of-freedom driving simulator subject to perturbation, Simulation 91 (3) (2015) 265–275.

[14] B. Achili, B. Daachi, Y. Amirat, A. Ali-cherif, A robust adaptive control of a parallel robot, Int. J. Control 83 (10) (2010) 2107–2119.

[15] E. Yime, R. Saltaren, J. Diaz, Robust adaptive control of the Stewart-Gough robot in the task space, Proceedings of the American Control Conference (ACC), IEEE, 2010, pp. 5248–5253.

[16] A. Salimi Lafmejani, M. Tale Masouleh, A. Kalhor, Position control of a 6-dof pneumatic Gough-Stewart parallel robot using backstepping-sliding mode controller, Mod. Mech. Eng. 17 (10) (2017) 101–111.

[17] N. Andreff, P. Martinet, Unifying kinematic modeling, identification, and control of a Gough–Stewart parallel robot into a vision-based framework, IEEE Trans. Rob. 22 (6) (2006) 1077–1086.

[18] S. Briot, V. Rosenzveig, P. Martinet, E. Özgür, N. Bouton, Minimal representation for the control of parallel robots via leg observation considering a hidden robot model, Mech. Mach. Theory 106 (2016) 115–147

[19] R. Hao, J. Wang, J. Zhao, et al., Observer-based robust control of 6-DOF parallel electrical manipulator with fast friction estimation, in: IEEE Transactions on Automation Science and Engineering, 2016, 13(3), pp. 1399-1408.

[20] H. Peng, J. Wang, W. Shen, et al., Cooperative attitude control for a wheel-legged robot, in: Peer-to-Peer Networking and Applications, 2019, 5(1), pp. 1-12.

[21] D. Shi, J. Wang, Y. Huang, et al., Event-triggered active disturbance rejection control of DC torque motors, in: IEEE/ASME Transactions on Mechatronics, 2017, 22(5), pp. 2277-2287.

[22] D. Shi, J. Xue, J. Wang, et al., A high-gain approach to event-triggered control with application to motor systems, in: IEEE Transactions on Industrial Electronics,2019, 66(8), pp. 6281-6291

Declarations

Availability of data and materials

Not applicable.

Competing interests

The authors declare that wo do not have any commercial or associative interest that represents a conflict of

interest in connection with the work submitted. Thank you very much for your time and consideration.

Funding

This study was supported by Nation Natural Science Foundation of China under Grant 61773060.

Authors' contributions

Professor Wang Shoukun developed the idea for the study, Dr.Chen Zhihua helped the translations of world, analysed the data, Mr.Liu Daohe conceived the study, designed the study and wrote the initial draft of the paper. All authors contributed to refining the ideas, carrying out additional analyses and finalizing this paper.

Acknowledgements

First and foremost, I would like to show my deepest gratitude to my supervisor, Professor Wang Shoukun, a respectable, responsible and resourceful scholar, who has provided me with valuable guidance in every stage of the writing of this thesis. His keen and vigorous academic observation enlightens me not only in this thesis but also in my future study.

Second, I would like to express my heartfelt gratitude to Dr.Chen Zhihua, who led me into the world of translation. I am also greatly indebted to the professors and teachers at the Laboratory, who have instructed and helped me a lot for this article. I shall extend my thanks to Professor Wang Junzheng for all her kindness and help. I would also like to thank all my teachers who have helped me to develop the fundamental and essential academic competence.

Last my thanks would go to my beloved family for their loving consideration and great confidence in me all through the writing.

Figures

Figure 1

Parallel structure of six wheel-legged robot

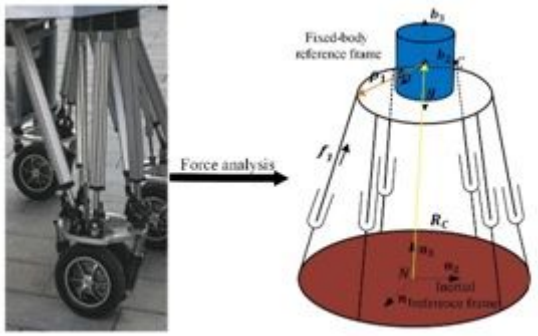

Figure 2

Force analysis of leg with load

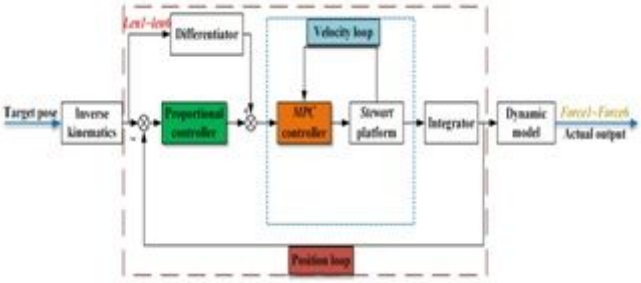

Figure 3

Control diagram of single leg

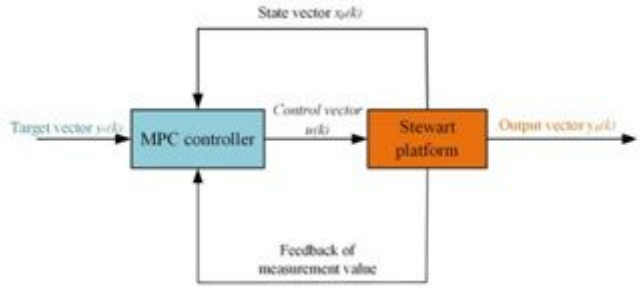

Figure 4

MPC controller and velocity loop control

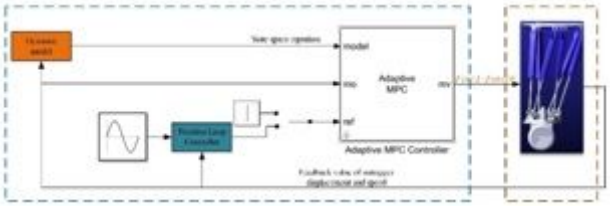

Figure 5

Control block diagram in Simulink

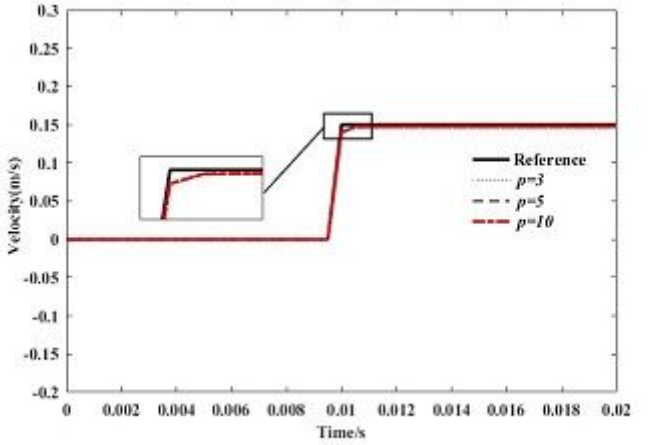

(a) Step response for m=2 and variable p

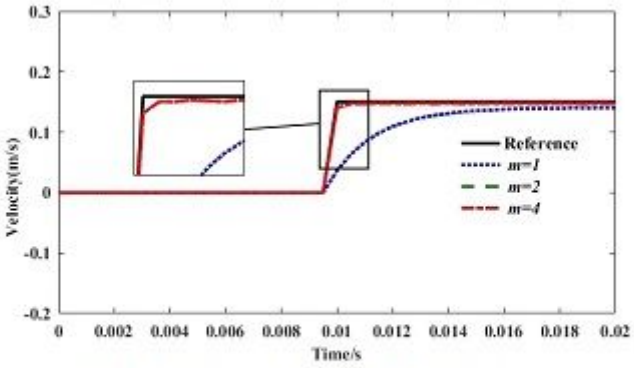

(b) Step response for p=5 and variable m

Figure 6

Step response for variable p and m

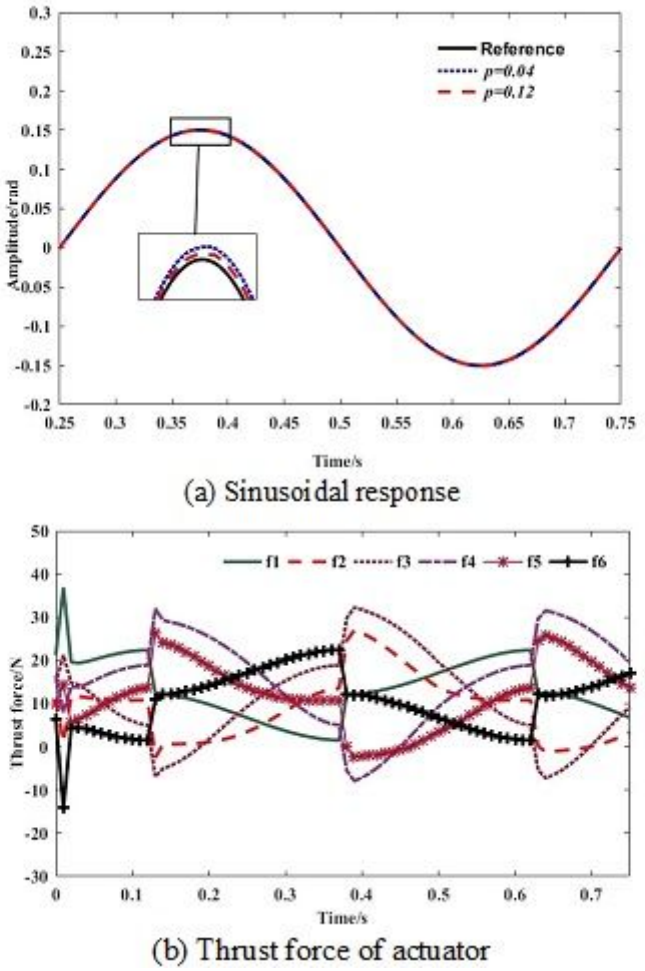

Figure 7

Sine wave response for m=2,p=5

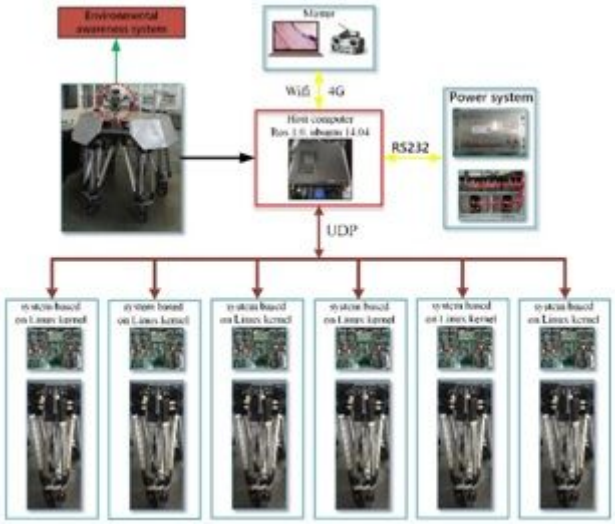

Figure 8

Framework of robot distributed system

Figure 9

Trajectory tracking of the single leg

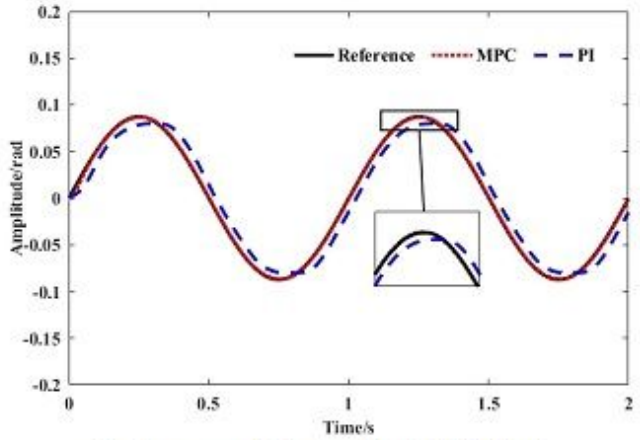

(a) Frequency 1Hz, Amplitude 0.0873Rad

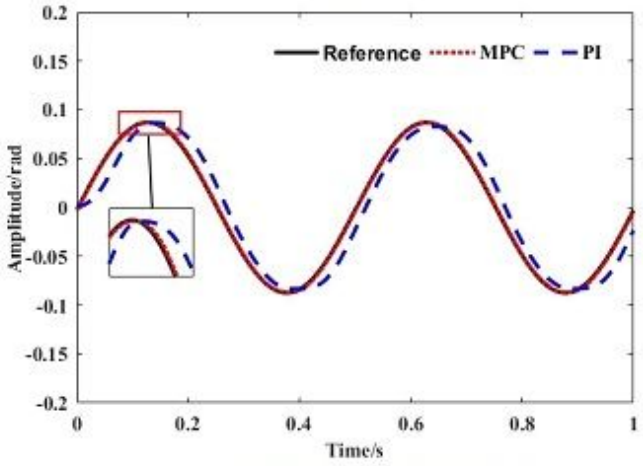

(b) Frequency 2Hz, Amplitude 0.0873Rad

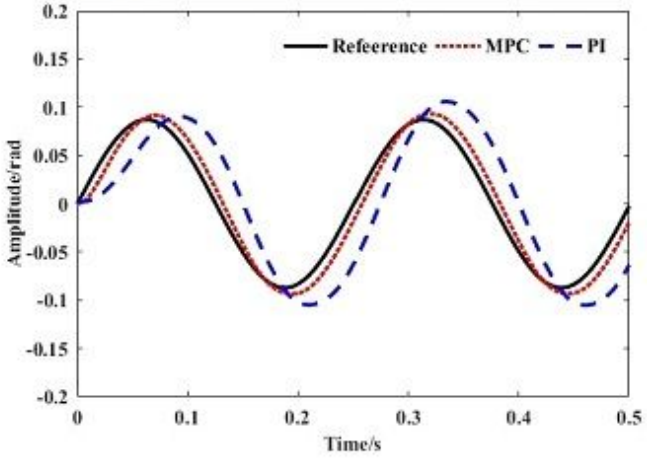

(c) Frequency 4Hz, Amplitude 0.0873Rad

Figure 10

Attitude tracking comparison between MPC controllerand PI controller

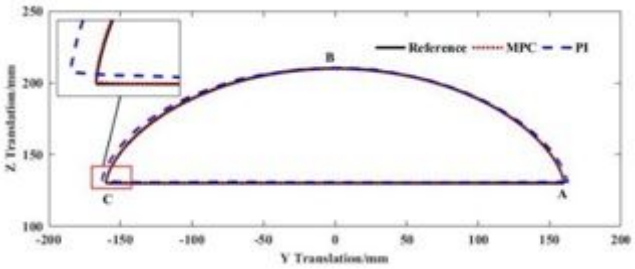

Figure 11

Displacement tracking comparison between MPC controller and PI controller